Hyperspectral Image Anomaly Targets Detection with Online Deep Learning

Ning Ma, Yu Peng, Shaojun Wang, Datong Liu
School of Electrical Engineering and Automation
Harbin Institute of Technology (HIT)
Harbin, China
Email: wangsj@hit.edu.cn

Abstract—Hyperspectral image (HSI) anomaly targets detection has been widely used in disaster alarm and military applications. Deep learning based HSI anomaly detector (AD) performs better by learning high-level features. However, the issues from heavy training computational burden and the model mismatch bring new challenges for online applications in the aspect of processing speed and detection accuracy. In this paper, an online Maximum-Distance-Pixel-Library(MDPL) method is proposed by using the most effective pixels to update deep auto-encoder based HSI AD with less extra computation. Experimental results on two recorded hyperspectral images show that the proposed method outperforms the traditional real-time local Reed-Xiaoli based detector in term of accuracy and processing time. Compared with fully updating deep learning based HSI AD, the proposed method performs higher time efficiency without accuracy loss.

Index Terms—Hyperspectral image, anomaly detection, on-board processing, online deep learning

I. INTRODUCTION

With hundreds of very narrow spectral bands, hyperspectral image(HSI) can identify the material of objects [1]. Because of the wide application scenarios, HSI anomaly detection has gain growing interest from researchers [2].

In general, an anomaly target in HSI is defined as an object or pixel which is different with most of the other pixels in term of spectral signature [3], such as a ship on the sea. In most of the monitoring applications, the detection along with image collection is usually required. Because the earlier alarm information is received, the more effective operations can be taken before disaster bursting. Such as fire monitoring in the forest, the detection result is expected to be received in a negligible time after data collection. In general, a tolerable delay may range from one to tens of seconds depending on application requirements. So some of the HSI ADs are implemented onboard to overcome the data link delay to realize online or real-time detection. But the processing is usually limited by onboard computer's performance.

Among the HSI ADs, a widely studied algorithm is RXD, which was proposed by Reed-Xiaoli [4] in 1990. The basic assumption for RXD is that the image should follow n the Gaussian distribution. By calculating the distance between pixel under test (PUT) and the background, the anomalies can be identified. RXD is widely used as baseline algorithm. As for

real-time anomaly detection mission, in 2014, Shih-Yu Chen [5] proposed a real-time causal RXD based HSI AD (RT-CK-RXD). Then, in 2017, Weiwei Deng [6] proposed a real-time local RXD based HSI AD (BLRXD) which calculates causal sample covariance matrix and updates the covariance matrix with Woodburys lemma. However, the image distribution assumption requirement from RXD based AD may not always be well met in real HSI AD applications, which may decrease the detection accuracy.

Recently, deep learning based HSI processing methods have received more attention. They have been proved to better extract the high level spectral and spatial features from HSI data [7], [8]. In 2016, Emrecan Bat [9] proposed a deep auto-encoder HSI AD which encodes the HSI pixel into a sparse code to represent the high-level features of the complex background. Then the reconstruction errors are calculated by decoding the code image and regarded as anomaly score to identify the anomalies. Based on similar principle, a DBN reconstruction errors based HSI AD was proposed in Ref [10] to improve accuracy as well. In 2017, Chunhui Zhao [8] proposed a stacked denoising autoencoders based method to learn high-level features from the hyperspectral image to overcome the detection accuracy decline by the impact of noise and nonlinear correlation on spectral information. However, in real-time onboard detection applications, the camera platform (such as satellite) flies over different kinds of ground scenes, the HSI dataset features may change. For deep learning based HSI AD, the change of features may lead to model mismatch and cause the false alarms.

To fix model mismatch in real-time applications, following challenges should be carefully considered.

1) The model should be updated according to the newly input data to better adapt to the new features. In addition, for better accuracy, the previous samples' features should be contained in HSI AD during model updating to keep global features of HSI.

2) To realize real-time detection, fewer samples are expected for model update. It is a contradiction to get high detection accuracy with less samples. Therefore, an efficient model update strategy needs to be elaborately managed to balance them.

In this paper, a deep auto-encoder based Maximum-Distance-Pixel-Library (MDPL) algorithm is proposed to realize an online HSI AD. With auto-encoder network, the anomalies can be identified according to the reconstruction error. A large reconstruction error usually means anomaly or features change. That is the basic principle of our AD. Once the feature change is detected, the model will be updated. In order to reduce the update computation load, we only select part of the newly input pixels by MDPL algorithm instead of all the pixels. In MDPL, we judge a new pixel whether it should be added to the update sample library according to its distance with neighboring pixels. The main contributions of this paper are summarized as follow:

1) To the best of our knowledge, we first proposed the deep auto-encoder combined with maximum distance pixel library(MDPL) algorithm to realize online HSI anomaly dectection.
2) To reduce the computation burden without accuracy loss, a continuous parameters update method is proposed for SAE based HSI AD to keep the global features of HSI dataset.

The remainder of this paper is organized as follows: In section II, the basic methodology of SAE and weight based HSI AD is described briefly. In section III, the proposed model updating strategy is introduced in detail. Experiments on two real HSI dataset are used to verify the proposed algorithm in section IV. A brief conclusion is given in section V.

II. METHODOLOGY

In this section, an auto encoder based local HSI anomaly detector is described briefly which is used to extract the feature of HSI dataset and to give the reconstruction errors for each pixel. Then, a local distance based discriminating method is employed to identify the anomaly targets.

A. Deep Auto Encoder Network

A deep autoencoder network is stacked by several neural networks with a symmetrical structure, such as deep belief network(DBN), stacked auto-encoder(SAE). A basic structure of the deep auto-encoder is given in the figure 1. The layers which contain a certain number of neuron points are connected by connection weights. For each neuron, it maps the non-linear relation between its input and output by the activation function. In general, the activation function is described as a formula 1 which is named sigmoid function.

$$f(z) = \frac{1}{1 + exp(-z)} \tag{1}$$

The output of neurons in the $(l+1)$-th layer is defined as $a^{(l+1)}$ or $h_{W,b}(x)$ in formula 2a and 2b,

$$z^{(l+1)} = W^{(l)}a^{(l)} + b^{(l)} \tag{2a}$$

$$h_{W,b}(x) = a^{(l+1)} = f(z^{(l+1)}) \tag{2b}$$

where W is the connection weight. b denotes the bias of the l-th layer. Both of them are updated during the training.

In order to achieve unsupervised learning of the features from HSI dataset, the first layer and the output layer are set with the same neurons number. After training the network by minimizing the loss function with gradient descent [11], the network operates as an auto-encoder. For SAE, the loss function is defined as formula 3,

$$J(W, b) = \frac{1}{2m} \sum_{i=1}^{m} \left\| h_{W,b}(x^{(i)}) - y^{(i)} \right\|^2 + \frac{\lambda}{2} \sum_{l=1}^{n_l-1} \sum_{i=1}^{s_l} \sum_{j=1}^{s_{l+1}} \left(W_{ji}^l \right)^2 \tag{3}$$

where λ is weight decay parameter, m is the number of training samples, y denotes the decoding output of the network, n_l is the total layer numbers of the network, s_l is the neuron number of l-th layer.

Each pixel of HSI is applied as an independent sample and fed into the auto-encoder network for training and detecting. Different spectral bands of each pixel are directly fed to different neurons in input layer. For a new PUT, after encoding and decoding, the neuron values in the middle layer are saved as image code. The difference between PUT and its decode value is defined as reconstruction error, named $RecErr$.
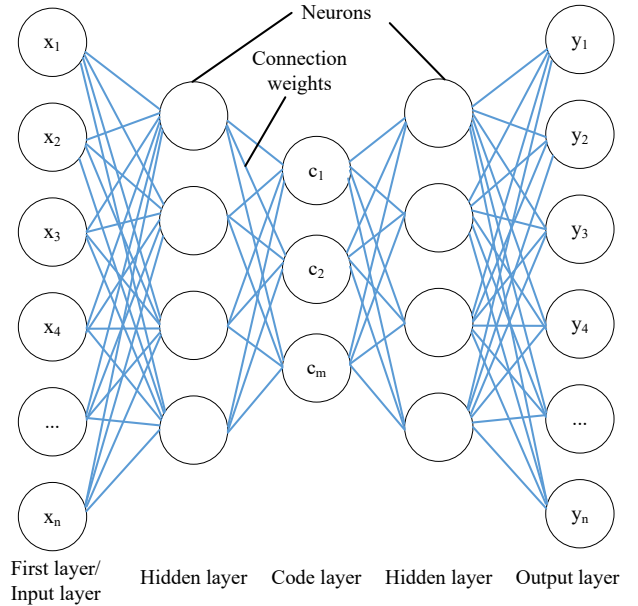

Fig. 1: The symmetrical structure of auto-encoder network.

The SAE network structure of proposed method is shown in figure 1. It was made up of five layers, and the neurons number of first and last layers are the same with the HSI spectral bands number. To realize sparse encoding, hidden layer size is less than spectral bands.

B. Local Weight based HSI AD

In order to identify anomaly pixels, a local weight based anomaly detector is introduced as follows. A dual window [12]–[14] centered on the PUT is built up to generate neighboring pixels as in figure 2. Then, anomaly score of the PUT is measured by the distance between PUT and neighboring pixels. The anomaly score δ_d is defined as in formula 4.
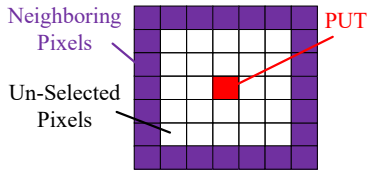
Fig. 2: Dual window method to generate local pixels.

$$\delta_d = 1/K \sum_{j=1}^{K} wt_j (\sum_{i=1}^{D} |x_{ji} - y_i|^2)^{1/2}, \qquad (4)$$

where K is the total number of local neighboring pixels, wt is the weight of local pixel which is reciprocal of its reconstruction error.

A greater anomaly score of a pixel means that this pixel has higher probability to be an anomaly object.

III. PROPOSED INCREASING LEARNING METHODS

For onboard HSI AD, with the moving of the camera, the features of HSI will change when different kind of ground scenes are collected. To describe the HSI dataset better, the features of the new scene need to be updated to HSI AD model to fix mismatch problem during detection. However, due to the limitation of onboard computing performance and the short detection delay requirement, just part of the new pixles can be selected out for model update to lower extra computation load without lossing accuracy loss. Considering the model mismatch is induced by the scene feature changing, so one key factor in new sample pixel selecting is to get the new features be contained. The sample selecting and the online detection method is proposed as shown in figure 3.
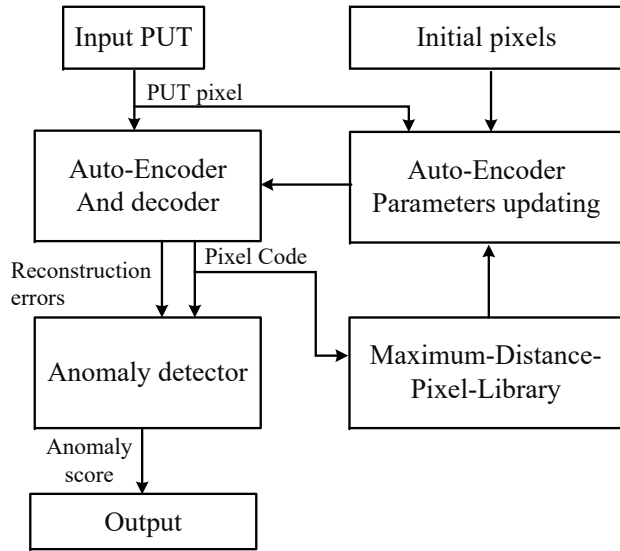

Fig. 3: The structure of proposed methods.

Before the anomaly detection, to initialize the connection parameters and bias of the SAE, a quick training is executed

with a small size of initial pixels. The initial pixels can be the pixels which are collected before the detection.

During the detection, the HSI pixels which are acquired continually are fed to the auto-encoder one by one. According to section II-A, the pixel code which is the output value of neurons in the middle layer is generated by the SAE network. To calculate the anomaly score in the formula 4, the neighboring pixels in the figure 2 are fed to the autoencoder to generate their pixel codes and reconstruction errors. The anomaly score is used to identify the anomaly targets.

Since the pixel code can stand for the features of the pixel, and reduce detection computation load with shorter data width than spectral bands. The pixel code is stored in MDPL for measuring the distances between new PUT and pixels in MDPL. In general, if a PUT contains new features, its average distance will be greater than others in MDPL. The average distance is calculated by the formula 5. This principle is used to determine which pixels should be used to update the auto-encoder model.

Before the detection, the MDPL is empty. The pixel code of the first PUT is added in MDPL, and its average distance is set to 0.

$$Dist_{th}^{(PUT)} = \frac{1}{k} \sum_{i=1}^{k} \left(\left\| \sum_{j=1}^{k} x_j^{(i)} - x_j^{(PUT)} \right\|^2 \right)^{1/2} \qquad (5)$$

where k is the number of pixel code in MDPL, $x_j^{(i)}$ and $x_j^{(PUT)}$ are the j-th dimension value of i-th pixel code in MPDL and the PUT pixel code, respectively. To further decrease the computation in updating, only the PUT whose average distance $Dist_{th}^{(PUT)}$ is larger than the maximum distance in MDPL is selected to update the model. The average distance and the pixel code selected PUT are added into MDPL for next PUT checking.

In order to fix model mismatch, new features are updated to the SAE model when a new PUT is determined for MDPL. To keep the global features of the detected HSI scene, the SAE model is updated by a forward propagation and a backward propagation train without re-initial. Such train method can perform almost the same accuracy with all the pixels being used to update the model.

IV. EXPERIMENTS

A. Dataset for experiments

The proposed HSI AD are evaluated by two real HSI dataset. The first HSI dataset was collected by the Airborne Visible Infrared Imaging Spectrometer (AVIRIS) on Caminada Bay in May 2010, which is embedded several image blocks as anomaly targets. The image was downloaded from NASA[1], the file f100524t01p00r09. A part of this dataset with the size of 1000×500 image is selected as a test image. The spatial resolution is 12.2m, and the spectral band number is 224. To

[1]http://aviris.jpl.nasa.gov/

synthetic anomaly targets, 4×4 image blocks are mixed with the ship pixel and the background average pixel in 20%, 40%, 60%, 80%, respectively. Each pixel of the test image is used as independent samples for the detector. The spectrum of above different anomaly pixels and background pixels are shown in figure 5, the data in different wavelength are used as the input for different layer neurons. The different lines in figure 5 are the spectrum signature for different targets including the average spectrum of background pixels. Then, 44 image blocks are embedded to test image. In test image, 30% value of the pixels which will be replaced by blocks is kept. The remain 70% value of the pixels is filled with the value of the blocks. The fake color image and the ground truth image are shown in figure 4.

The second HSI dataset was collected by AVIRIS over San Diego airport [8], 126 spectral bands are used to validate the proposed anomaly detector. There are 38 planes which are regarded as anomaly targets, its color image and the ground truth image are shown in figure 6.

The ground truth image is used to indicate the location of anomaly targets in where the pixel value is labeled as 1 and display as white pixels in figure 4 and in figure 6 . Meanwhile, the background is marked as 0 and display as black pixels in the figures. The detection results for each pixel will be compared with ground truth image to verify the accuracy of the proposed method.

To validate the proposed methods, two test images are employed, and 500 thousand independent samples in first test image and 10 thousand independent samples in second test image are used.

To appraise the proposed method, real-time local RX based HSI AD(BLRXD) is performed on the test image as benchmark algorithm, and a full updating SAE HSI AD which updates the SAE network at the end of each PUT detection is employed on the test image as well.
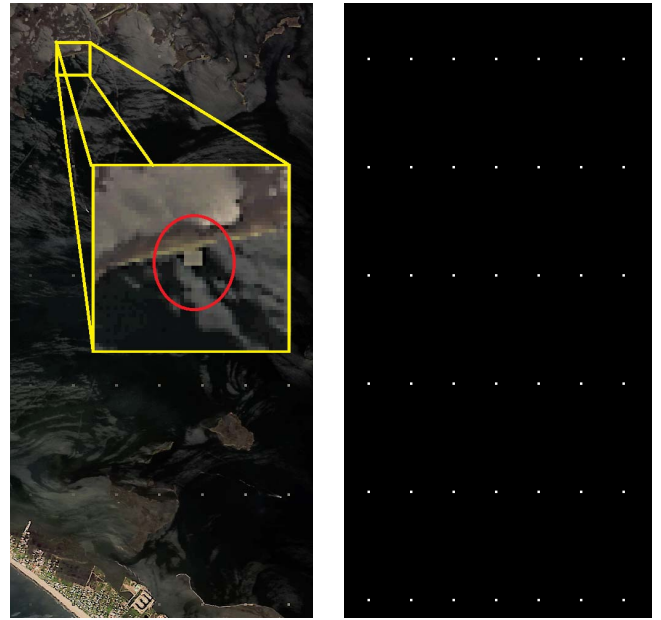
B. Experimental environment and the evaluation criteria

The experiments are run with Matlab 2016b on AMAX workstation with two Intel E5-2640v4 processors. To evaluate the proposed method, the receiver operating characteristic (ROC) curve and the area under the ROC curves (AUC) [15] are used in term of detection accuracy. The detection time is measured to analyze the time efficiency.

C. Results and discussion

The structure of SAE network in MPDL depends on the spectral bands number of the test image dataset because the neurons number in the first and last layer should be same as the spectral number. For the first test image, the neurons number from the first to the last layers in the SAE structure are 224,180,2,180,224 respectively, and for the second test image the layer size is 126,40,20,40,126. respectively.

A real-time local RX based hyperspectral anomaly detector (BLRXD) [6] is employed for comparison. In BLRXD, an unsuitable size of the local window may break the assumption of the local Gaussian distribution or make the correlation

(a) The fake color image of test image.

(b) The position of embedded synthetic anomaly blocks in test image

Fig. 4: The test image and the embedded anomaly targets on Caminada BAY.
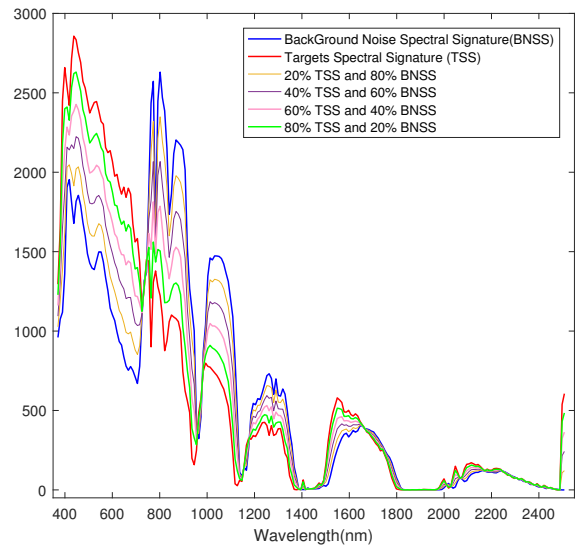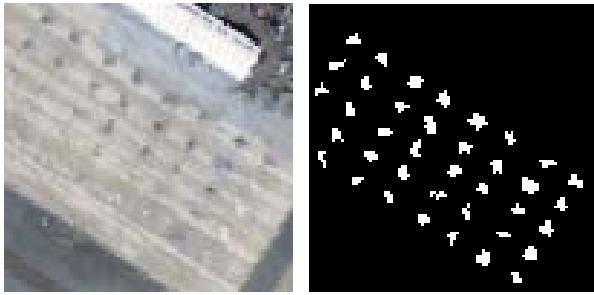

Fig. 5: The spectrum of embedded anomaly targets and the background

matrix become a singular matrix, and degrade the detection performance. In this paper, a searching for the local window size from 15×15 to 65×65 is executed (mainly to avoid the matrix singular). The smallest one is 60×60 to keep the correlation matrix from the singular matrix for better detection accuracy. For second test HSI image. After optimization, the local window size is set to 26×26 for the best detection

(a) The fake color image of San Diego airport HSI

(b) The ground truth of San Diego airport.

Fig. 6: The test image and anomaly targets on San Diego airport.

accuracy.

Different threshold for anomaly score lead to different False Positive Rate(FPR) and Truth Positive Rate(TPR), by change the threshold from the minimum anomaly score to the maximum anomaly score, and comparing the identifying results to the ground truth, the ROC curve of proposed method, the full updating SAE HSI AD and the BLRXD method are drawn in figure 7 and in figure 8 for two test images respectively, and the AUC value and the executing time are shown in Table I and Table II.
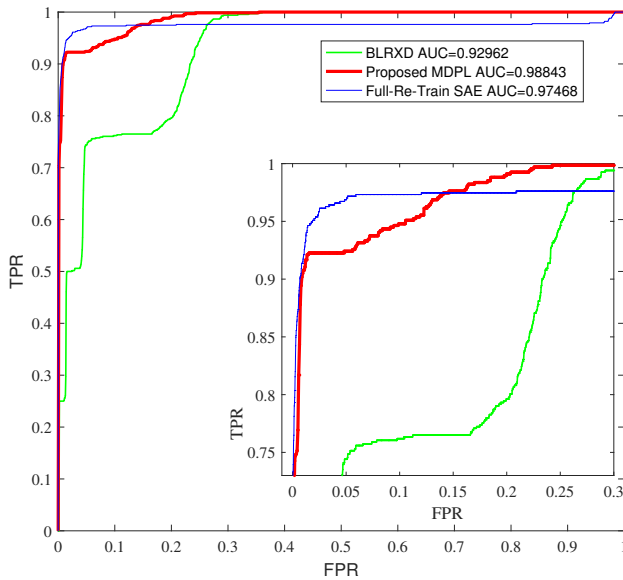

Fig. 7: The ROC curve results Caminada BAY test image

From Table I and Table II, the proposed MDPL AD outperforms the local real-time RX based HSI AD (BLRXD) in term of AUC value and the executing time. It is because that the transcendental function in each neuron of MDPL AD can map the non-linear characters of HSI dataset without Gaussian distribution assumption. Moreover, with the help of weight-

TABLE I: AUC values and detection time of Caminada BAY test image.

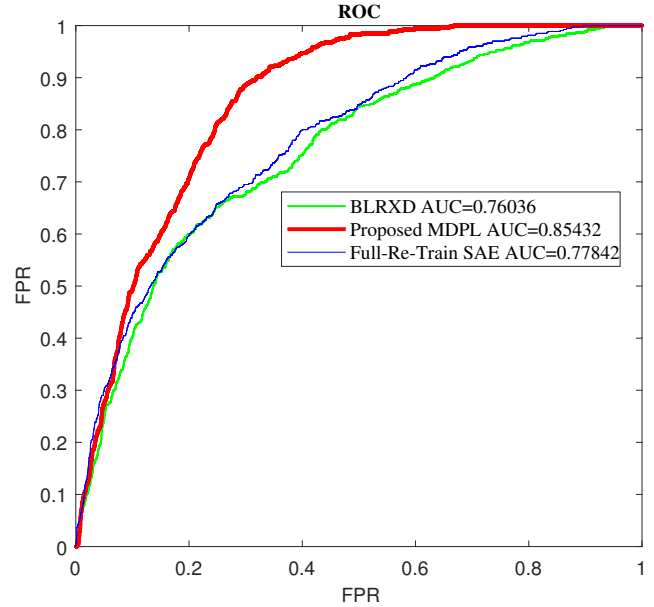| Detector Name	AUC Value	Executing time(s)
Proposed MDPL AD	0.9884	262.5
SAE without MDPL AD	0.9747	1217.6
Real-time local RXD(BLRXD) [6]	0.9296	2444.8

Fig. 8: The ROC curve results of San Diego airport test image

based local anomaly detection method in Section II-B, a high detection accuracy can be achieved. In view of detection time, due to small size window used in the proposed MDPL AD, less time is required. While in BLRXD, the huge number of local pixels requires more detection time. The proposed MDPL AD reach up to $3.3\times$ to $9.2\times$ time efficiency to BLRXD. Due to smaller local window size is used in BLRXD for the second test image, so less computation and less time is cost.

By analyzing the Maximum-Distance-Pixel-Library, only 51 new pixels are included to update the SAE model in the first test image. The proposed MDPL AD performs about $4.6\times$ time efficiency to full updating SAE HSI AD which employs 500000 pixels for updating in the first test image. For the second test image, the time efficiency is about $4.4\times$. The AUC value of the proposed MDPL AD is a little higher than full updating SAE HSI AD.
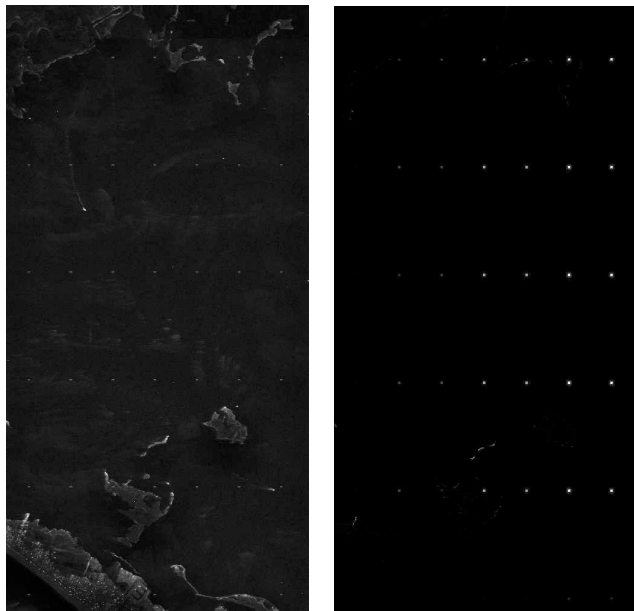
The grey image of anomaly score from proposed MDPL

TABLE II: AUC values and detection time of San Diego airport test image.

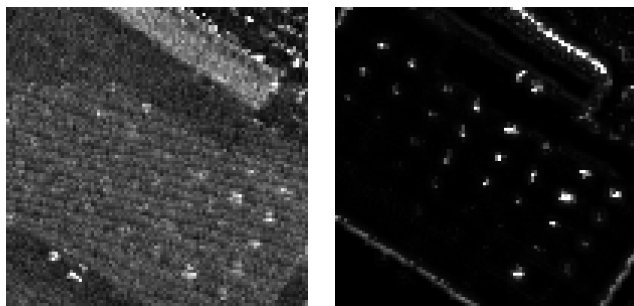| Detector Name	AUC Value	Executing time(s)
Proposed MDPL AD	0.8543	3.5
SAE without MDPL AD	0.7784	15.4
Real-time local RXD(BLRXD) [6]	0.7603	11.5

HSI AD and the BLRXD are shown in 9 and in 10. The brighter the pixel is, the higher probability as an anomalous pixel will be. As is shown in the results, the BLRXD gives the more false alarm in the border of two backgrounds, while the proposed MDPL performs well. Most of the background pixels are displayed in the same position with the groundtruth image, and the most of targets are clearly and right displayed in the grey image of proposed MDPL results.

Due to the proposed online model parameters update method well solves the model mismatch problem, the proposed MDPL AD outperforms better detection accuracy than classic BLRXD and the full updating SAE HSI AD. With the benefit of less updating times, the proposed method run over $3\times$ faster than BLRXD and full updating SAE HSI AD.

(a) The anomaly score grey image of BLRXD detector
(b) The anomaly score grey image of proposed MDPL detector

Fig. 9: The detection results in grey image of Caminada BAY dataset

(a) The anomaly score grey image of BLRXD detector
(b) The anomaly score grey image of proposed MDPL detector

Fig. 10: The detection results in grey image of San Diego dataset.

V. CONCLUSION

Online HSI AD is widely required in real applications. For deep learning based HSI AD which performs well in the offline mission, it is still a big challenge to overcome the model mismatch problem with less computational requirements in online application. In this paper, an online MDPL AD is proposed with less updating pixels by a maximum average distance strategy without accuracy loss. Experimental results on two real HSI datasets which have been embedded with anomaly targets show the proposed method reach up to 3.2 to 9.2 times speedup comparing to BLRXD and full updating SAE HSI AD respectively. It also gets better detection accuracy than the aforementioned comparison methods. In the future, a more efficient re-training pixel selection method needs to be further studied to overcome the problem that the size of MDPL may increase along with detection time.

REFERENCES

[1] C.-I. Chang, "Hyperspectral target detection," in *Real-Time Progressive Hyperspectral Image Processing*. Springer, 2016, pp. 131–172.

[2] G. Healey and D. Slater, "Models and methods for automated material identification in hyperspectral imagery acquired under unknown illumination and atmospheric conditions," *IEEE Transactions on Geoscience and Remote Sensing*, vol. 37, no. 6, pp. 2706–2717, 1999.

[3] C.-I. Chang, Y. Li, M. C. Hobbs, R. C. Schultz, and W.-M. Liu, "Progressive band processing of anomaly detection in hyperspectral imagery," *IEEE Journal of Selected Topics in Applied Earth Observations and Remote Sensing*, vol. 8, no. 7, pp. 3558–3571, 2015.

[4] I. S. Reed and X. Yu, "Adaptive multiple-band cfar detection of an optical pattern with unknown spectral distribution," *IEEE Transactions on Acoustics, Speech, and Signal Processing*, vol. 38, no. 10, pp. 1760–1770, 1990.

[5] S.-Y. Chen, Y. Wang, C.-C. Wu, C. Liu, and C.-I. Chang, "Real-time causal processing of anomaly detection for hyperspectral imagery," *IEEE Transactions on Aerospace and Electronic Systems*, vol. 50, no. 2, pp. 1511–1534, 2014.

[6] Z. Chunhui and D. Weiwei, "Hyperspectral anomaly detection algorithm by using recursive polynomial function," *Journal of Shenyang University (Natural Science)*, vol. 1, p. 006, 2017.

[7] L. Zhang, L. Zhang, and B. Du, "Deep learning for remote sensing data: A technical tutorial on the state of the art," *IEEE Geoscience and Remote Sensing Magazine*, vol. 4, no. 2, pp. 22–40, 2016.

[8] C. Zhao, X. Li, and H. Zhu, "Hyperspectral anomaly detection based on stacked denoising autoencoders," *Journal of Applied Remote Sensing*, vol. 11, no. 4, p. 042605, 2017.

[9] E. Batı, A. Calıskan, A. Koz, and A. A. Alatan, "Hyperspectral anomaly detection method based on auto-encoder," in *Proc. of SPIE Vol*, vol. 9643, 2015, pp. 96 430N–1.

[10] N. Ma, S. Wang, J. Yu, and Y. Peng, "A dbn based anomaly targets detector for hsi," in *AOPC 2017: 3D Measurement Technology for Intelligent Manufacturing*, vol. 10458. International Society for Optics and Photonics, 2017.

[11] G. E. Hinton, S. Osindero, and Y.-W. Teh, "A fast learning algorithm for deep belief nets," *Neural computation*, vol. 18, no. 7, pp. 1527–1554, 2006.

[12] W.-m. Liu and C.-I. Chang, "Multiple-window anomaly detection for hyperspectral imagery," *IEEE Journal of Selected Topics in Applied Earth Observations and Remote Sensing*, vol. 6, no. 2, pp. 644–658, 2013.

[13] H. Kwon, S. Z. Der, and N. M. Nasrabadi, "Adaptive anomaly detection using subspace separation for hyperspectral imagery," *Optical Engineering*, vol. 42, no. 11, pp. 3342–3351, 2003.

[14] W. Li and Q. Du, "Decision fusion for dual-window-based hyperspectral anomaly detector," *Journal of Applied Remote Sensing*, vol. 9, no. 1, pp. 097 297–097 297, 2015.

[15] C.-I. Chang, "Multiparameter receiver operating characteristic analysis for signal detection and classification," *IEEE Sensors Journal*, vol. 10, no. 3, pp. 423–442, 2010.